Available online at www.sciencedirect.com
ScienceDirect
Cold Regions Science and Technology 47 (2007) 233–255
cold regions science and technology
www.elsevier.com/locate/coldregions

How fast is landfast sea ice? A study of the attachment and detachment of nearshore ice at Barrow, Alaska

Andrew Mahoney *, Hajo Eicken, Lewis Shapiro

Geophysical Institute, University of Alaska Fairanks, 903 Koyukuk Drive, Fairbanks, AK 99775–7320, United States

Received 28 July 2006; accepted 20 September 2006

Abstract

During the two winters between 2003 and 2005, a land-based marine radar observed the nearshore ice motion during the development and decay of landfast ice near Barrow, Alaska. The radar imagery captured individual events at high temporal resolution, revealing deformation processes and allowing calculation of ice velocity and acceleration. Atmospheric forcing during these events appeared to be irrelevant since no corollary was found in local meteorological observations. Detailed examination of the radar imagery showed that backscatter from sea ice targets oscillated in signal strength (flickered) prior to detachment, as previously observed by (Shapiro, L.H. (1987), Mechanical Properties of Sea Ice Deformation in the near Shore Zone, in OCSEAP Final Reports, V.72, pp. 357–584, U.S. Dept. of Commerce, NOAA). Determination of ice acceleration after detachment allowed estimation of water drag beneath the ice.

The distribution of grounded ridges at the end of each annual cycle was determined from field measurements of ice elevation, ice thickness and water depth. Applying a simple theoretical treatment of coupling between a first-year ridge keel and the seabed, we calculate that the anchoring strength provided by ridges was 2–3 orders of magnitude greater than typical wind or water stresses. Therefore, we conclude that additional decoupling processes, such as sea level surges or thermal erosion of keels, must occur in addition to offshore current stress in order to cause the landfast ice to detach. Although the nature of these processes is not clear, they are likely to be the cause of the flickering observed in radar imagery, which could therefore be useful in short-term prediction of detachment events.

Keywords: Landfast sea ice; Radar; Grounded ridges; Sea ice thickness; Anchoring strength

1. Introduction

Bordering the coastlines of ice-covered seas, landfast ice is the form of sea ice with which people have most frequent contact and has the most direct impact on human activities and lifestyles. For thousands of years, Arctic communities have used landfast sea ice to gain access to the marine mammals that frequent open water at its seaward edge and they have benefited from its presence to mitigate the erosional effects of winter storms. In more recent years, landfast ice has been used as a platform for conducting offshore oil and gas development.

Lack of motion and contiguity with the land are the common elements of numerous definitions of landfast ice (Mahoney et al., 2005) and are integral to the nature of landfast sea ice and people's interaction with it. However, satellite observations in northern Alaska indicate a reduced presence of landfast ice in recent

* Corresponding author.
E-mail address: Andrew.Mahoney@nsidc.org (A. Mahoney).

0165-232X/$ - see front matter © 2006 Elsevier B.V. All rights reserved.
doi:10.1016/j.coldregions.2006.09.005

years (Mahoney et al., in press). This is partly attributed to the earlier onset of thawing temperatures in spring and a later incursion of pack ice into coastal waters in fall as a result of recent increases in the northward retreat of the perennial ice edge (Serreze et al., 2003; Stroeve et al., 2005). These observations agree with those of indigenous communities around the Arctic who note that recently landfast sea ice is less stable, forms later and breaks up earlier than in the past (Fox, 2002; Jolly et al., 2002; George et al., 2004). In addition, there have been an apparently unusual number of mid-season break-outs in recent years that have endangered hunters who became stranded from the land (MacDonald, 2002; Norton and Graves Gaylord, 2004).

With increasing shipping and mineral exploration interest in Arctic coastal waters, understanding the processes behind these changes in landfast ice behavior is becoming more important. However, the mechanisms that hold the ice fast and the balance of forces that act upon it are not well known. This is partly due to the difficulties involved in observing the brief episodic events that shape the ice cover, which often occur during inclement weather or darkness and incur significant risk to ice-based instruments. In this study we begin with a theoretical treatment of the attachment of sea ice to land. Then, analyzing two years of land- and ice-based observations of the landfast ice near Barrow, Alaska, we examine the break-up and detachment events in the context of the whole annual cycle. In doing so, we elucidate the processes responsible for fastening and unfastening of landfast sea ice.

2. Attachment to the coast

The majority of landfast ice is floating and therefore held in place by non-floating landfast ice, of which there are two main kinds: bottomfast ice and grounded ice. Bottomfast ice exists where the water depth is shallow enough that the sea ice grows and freezes to the seabed (Reimnitz and Barnes, 1974; Reimnitz, 2000). To accommodate the differential motion between bottomfast and floating ice caused by changes in sea level, a tide crack forms near the beach. This tide crack appears to be a ubiquitous feature of the northern Alaskan landfast ice (Kovacs and Mellor, 1974; Reimnitz and Barnes, 1974; Reimnitz, 2000) and presumably has little tensile strength. Therefore, it is doubtful that bottomfast ice plays a significant role in attaching floating landfast ice to the land along open coasts or beyond barrier islands, although it could be important in highly convoluted embayments or shoreward of barrier islands.

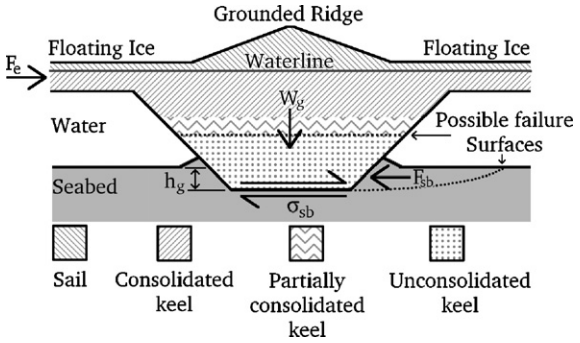

Fig. 1. A generalized cross-section of a grounded first year ridge fragment parallel to direction of ungrounding force. Note that the orientation of the cross-section is arbitrary relative to the axis of the ridge, the coastline or gouged trench (if present). In the case where the ungrounding force acts backwards along the direction of gouging there may be no gouge wall to provide the seabed force, F_{sb}. See text for explanation of terms.

This study focuses on an open section of coast in the vicinity of Barrow, where the floating landfast ice is held in place by grounded ridges. These ridges can either drift into shallow water from offshore or form through in situ deformation of sea ice such that their keels reach the sea floor. Elsewhere, ice islands can also become incorporated into landfast ice, but this is not a common occurrence in northern Alaska. Each grounded ridge provides anchoring strength to the surrounding landfast ice, which will be limited by either the strength of the ridge's keel or its coupling with the seabed.

First-year ridges, which comprise the majority of ridges in northern Alaskan landfast sea ice (at least under present-day conditions with the perennial sea ice typically retreating far to the North), have keels composed of consolidated, partially consolidated and unconsolidated rubble (Pilkington et al., 1980; Leppäranta and Hakala, 1992; Leppäranta et al., 1995; Blanchet, 1998; Høyland and Løset, 1999; Høyland, 2002) (Fig. 1). For anchoring landfast ice, it is the shear strength of the unconsolidated keel that is of interest, which full-scale tests show to be highly variable. Although many test results are proprietary, Leppäranta and Hakala (1992) measured unconsolidated shear strength values between 1.7 and 4.0 kPa, while Croasdale et al. (2001) measured values between 6 and 23 kPa, with a mean of 14.1 kPa. Croasdale et al. (2001) also found some indication of increasing shear strength with keel size, but changes in consolidation and porosity over time caused by wintertime freezing and spring melting also affect keel shear strength (Høyland and Løset, 1999; Høyland, 2002).

Coupling between the ridge keel and the seabed results from shear stress due to friction at the keel–bed interface and a gouging force required to move any

material from in front of the keel (Fig. 1). The shear stress at the seabed, σ_{sb}, is given by:

$$\sigma_{sb} = \frac{W_g c_f}{A_g} \quad (1)$$

where W_g is the grounded weight of the ridge, taking account of buoyancy, c_f is the coefficient of friction between the seabed and ice and A_g is the area of ice in contact with the seabed. For simplicity, we assume a smooth keel and ignore the effects of individual blocks gouging the seabed. By physically dragging blocks of ice up the beach at Barrow, Shapiro and Metzner (1987) derived a value for c_f of 0.5 for static friction. Due to its dependence on W_g, frictional seabed coupling is clearly sensitive to changes in water level.

Seabed gouging often occurs during the grounding process, especially in the case of ridges created offshore that become grounded by drifting into shallow water. Unless the ridge is being forced in the direction from which it came, the keel will have to re-gouge the seabed if it is to move. Gouging forces have been studied extensively in the interests of designing seafloor pipelines in ice-covered seas and a number of numerical models have been developed (e.g. Been et al., 1990; Marchenko, 2003; Croasdale et al., 2005; Marchenko, 2005; Phillips et al., 2005).

It is beyond the scope of this study to fully model gouging forces, which will depend upon the steepness and cross-section of the gouging keel as well as the density, porosity and cohesion of the seabed. However, Phillips et al. (2005) present predictions from the Pressure Ridge Ice Scour Experiment (PRISE) model of the horizontal force required for given depth of gouging. These include components of frictional resistance and a passive seabed force (F_{sb} in Fig. 1) and can be approximated by quadratic functions of gouge depth, h_g, if we assume that the overall force depends upon two properties: first, the cross-section of the gouging keel, which is linearly proportional to h_g; second, the confining pressure on the seabed, which is proportional to the size of the ridge, which also has a linear relationship with h_g (Phillips, pers. comm., 2006).

Phillips also points out that the PRISE model predictions will typically over-estimate the force required to unground a grounded ridge. This is due to the model assumption of a steady state in which the seabed has rounded off the gouging face of the keel. In ungrounding a ridge that has gouged the seabed, the new gouging face is most likely to be steeper and therefore apply less downward confining stress to the seabed. In addition, assuming the ridge moves into deeper water, the gouging forces will decrease over time. Using these assumptions, a quadratic curve was fitted to the lower estimate of the PRISE model predictions to derive the following equation for estimating re-gouging force, F_g:

$$F_g = 0.2h_g^2 + 0.7h_g \quad (2)$$

where h_g is the depth of the gouge in which the ridge is grounded and F_g is expressed in MN m^{-1} of gouge length in contact with the ridge. F_g is limited by keel size and shear strength, which also limits h_g.

The overall anchoring strength that a grounded ridge can provide depends upon the strength of its keel and its interaction with the seabed during the grounding process.

For grounded ridges that do not rest in deep gouges, coupling with the seabed is sensitive to changes in sea level. This may be the case for ridges that are formed in situ or that have their keels sheared off during grounding. This could also conceivably apply to ridges being forced offshore in the direction of their gouge. However, a ridge that has gouged the seabed may be lifted from the seafloor by a rise in sea level, but prevented from moving horizontally by the walls of its gouge. The incorporation of such ridges into the landfast sea ice cover is a matter of timing, since ridges formed offshore will not be able to reach shallow water if a thick enough landfast ice cover already exists.

3. Methods

3.1. Land-based radar

A Raymarine 10 kW X-band (3.0 cm; 10 GHz) marine radar was installed at the Ukpeagvik Iñupiat Corporation

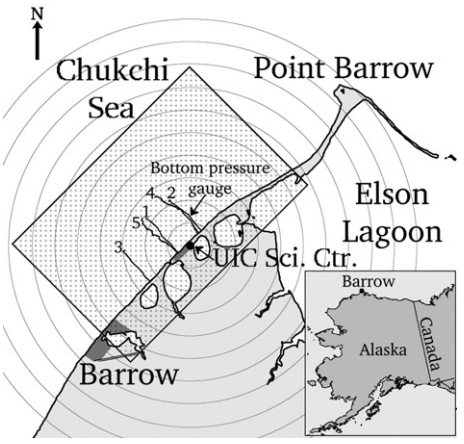

Fig. 2. Location and approximate effective range of the X-band radar deployed at the Ukpeagvik Iñupiat Corporation (UIC) Science Center near Barrow. Range rings are at 1-km intervals. The stippled box indicates the region for which radar imagery is shown in subsequent figures. The numbered lines indicate the locations of transects along which ice thickness and topography were measured (Section 3.2). The bottom pressure gauge is discussed in Section 3.3.

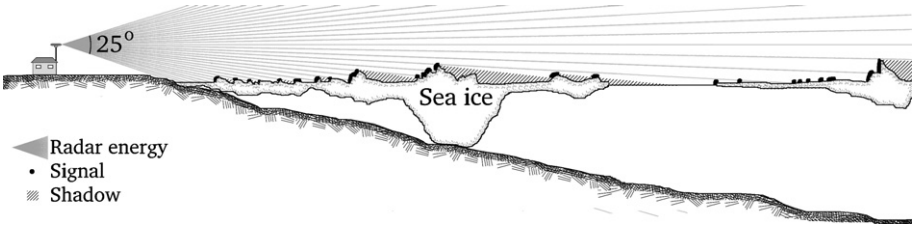

Fig. 3. Schematic illustration of landfast ice and the surface illuminated by the radar. Black dots show surfaces from which backscatter could be expected and cross-hatched areas indicate shadow zones from which no signal would be received.

(UIC) Science Center in Barrow (Fig. 2) in August 2003. A 48″ (1.22 m) open array antenna was used, which rotated at 30 rpm. The transceiver was mounted approximately 10 m above sea level and 50 m from the shoreline. The pulse length was 0.45 μs, which yielded a ground range resolution of approximately 67.5 m. The horizontal beam width of the antenna was 1.9°, which yields 165 m wide sampling area at a range of 5 km.

The signal received by the antenna depends upon the properties of the ice and the wavelength and grazing angle of the microwave energy. The signal will either be returned from the surface of the ice or from within its volume. The depth to which electromagnetic energy penetrates into a body is known as the skin depth. For X-band radar and sea ice, skin depth depends upon the bulk salinity and brine and therefore changes with the age and temperature of the ice. First year (FY) sea ice has a higher bulk salinity than multi-year (MY) sea ice and consequently has a thinner skin depth. Weeks and Ackley (1986) use the terms "high loss" to describe FY ice and MY sea ice respectively. Hallikainen and Winebrenner (1992) found skin depths of between 5 and 30 cm in FY ice and of up to several meters in MY ice. Field observations and satellite imagery suggest that the majority of sea ice in the field of view of the radar was FY ice, so we expect the radar returns that comprise the imagery in this study to come predominantly from the surface of the ice rather than the ice volume.

The microwave energy incident upon an ice surface will either be reflected in a specular manner away from the transceiver or scattered in many directions according to whether the surface is smooth or rough, respectively. This can be determined using the Rayleigh criterion (Haykin et al., 1994), which states that a surface is smooth if

$$h < \frac{\lambda}{8\sin y} \tag{3}$$

where h is the roughness height of the surface, λ is the wavelength of the radar and ψ is the grazing angle at which the radar beam impinges the surface.

It is important here to distinguish between grazing angles relative to a level surface and local grazing angles in the presence of ice topography (Fig. 3). The grazing angle over level ice and smooth water varies with the horizontal distance from the antenna such that the Rayleigh roughness height is linearly dependent upon the range from the radar. Due to the low elevation of the antenna, a radar beam will be reflected specularly from level ice and smooth water, except within a few hundred meters of the antenna. Any signal received by the antenna at greater distances will therefore come from topographic features that either satisfy the Rayleigh roughness criterion or provide a surface where the local grazing angle is great enough to allow smaller-scale roughness to scatter energy back to the transceiver. It is important to note that the absence of echoes does not imply a level surface however, since ice topography will result in shadow zones (Fig. 3).

The radar system used in this study was not specifically designed for scientific use and access to raw data was not possible. Instead, imagery was displayed as an orthorectified image on a personal computer screen using Raytech Navigator software. Data capture was accomplished by automated screen captures. In the first year of operation, screen captures were stored at 5-min intervals as Joint Photographic Expert Group (JPEG) images. In the second year of operation, images were stored every minute as Portable Network Graphic (PNG) images, but a fault with the radar's auto-tuning board degraded image quality, so consecutive images were combined to produce a single stacked image every 5 min.

The resulting effective pixel size was 18.5 m in all images, representing an oversampling of the signal. Built-in signal processing produced a color display with 3 colors (yellow, cyan and blue) that qualitatively indicated the strength of a return. However, the radar manufacturer states (Wolcott, 2005, pers. comm.) that there is no quantifiable relationship between the colors except that yellow indicates the strongest returns, while blue is close to the level of noise. For the analysis that follows, we excluded the cyan and blue pixels, which

together accounted for less than 2% of all pixels. This resulted in a binarized image of target pixels and non-target pixels. For this study, we refer to any contiguous area of target pixels as a "target". As stated above however, areas of non-target pixels do not necessarily represent smooth surfaces and other information must be employed to infer the nature of a surface from which no radar return is received.

Animating the imagery allowed more information to be deduced about the ice/water surface than is possible from a single image. For example, in an animated time-series, groups of targets often exhibit rigid body behavior, so that the area in between can be assumed to contain ice. Also, the presence of ice can be inferred in an area devoid of targets from convergence of targets around it. Similarly, divergence of targets implies lead formation and the presence of open water. In addition, the seaward boundary of the landfast ice can be identified when there is moving pack ice adjacent to the landfast ice. However, the absence of targets between the landfast ice and pack ice does not necessarily imply the existence of open water and may result from level ice or shadowing (Fig. 3). Animated radar imagery was used extensively in this study. This paper contains sequences of individual images that illustrate dynamic events (Sections 4.2–4.6). For a more complete appreciation of these events, we strongly encourage the reader to view animation files, which are available from http://www.gi.alaska.edu/snowice/sea-lake-ice/Data/SIR-Data_2003-05.html (address is case sensitive) or on DVD from the authors upon request.

Images were stored locally on the computer attached to the radar system and transferred across the Internet for archival and display in near-real-time on a website. This proved useful for monitoring the performance of the radar. However, due to a host of reasons related to operating a remote system with minimal supervision, the radar did not run continuously. Fig. 4 summarizes the availability of imagery from the land-based radar as well as the temporal coverage of other relevant data discussed in Sections 3.2–3.4.

3.2. Sea ice thickness and topography measurements

In order to estimate the fraction of grounded ridges in the landfast ice we made measurements of ice surface elevation and thickness along transects approximately perpendicular to the shore. We located these transects within the footprint of the radar for ground-truthing purposes. Ice thickness was measured by electromagnetic (EM) induction using a Geonics EM-31 Mk-II and by drilling. The EM-31 Mk-II is a ground conductivity meter that transmits a 9.8 kHz EM field to induce eddy currents in the ground beneath it, which in turn creates a secondary field. The strength of the secondary field is measured by the receiver coil and is directly proportional to the apparent conductivity, σ_a, or the volumetric distance-weighted mean conductivity of the ground over a footprint of a few meters. Since the conductivity of seawater is much greater than that of sea ice, apparent conductivity depends largely on the distance between the instrument and the ice–water interface.

In this study, we measured landfast sea ice thickness, H_i, during 4 different periods of field observation (periods B, C, D and H in Fig. 4). For each period, exponential functions of the form $\sigma_a = A_1 e^{A_2 H_i} + A_3$ were fitted to the data, following Haas and Eicken (2001) and Eicken et al. (2001). For transforming conductivity measurements into sea ice thicknesses, these were inverted to produce functions of the form $H_i = B_1 \ln(\sigma_a - B_2) + B_3$. Fig. 5 shows the data and the empirical formulae. Due to the logarithmic nature of the transformation functions, they each have asymptotes at $\sigma_a = B_2$, which can be interpreted as the apparent conductivity of an infinite slab of sea ice.

Data collected in May and June (field periods C, D and H) each exhibit similar asymptotes, while the data from February (field period B) exhibits an asymptote at a significantly higher value of σ_a. However, it should be noted that no ice thicker than 2.75 m was sampled during field period B. It should also be noted that during field period C, values of σ_a measured in thick, ridged ice are

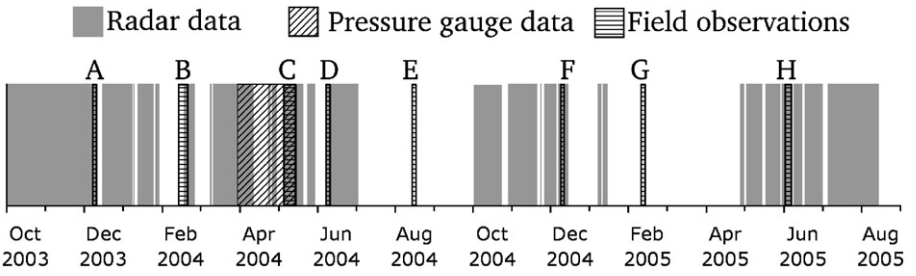

Fig. 4. Time line showing the time periods of observations by different methods. The letters identify separate periods of field observation. The measurements made during these are discussed in Sections 3.2–3.4. The pressure gauge is discussed in Section 3.3.

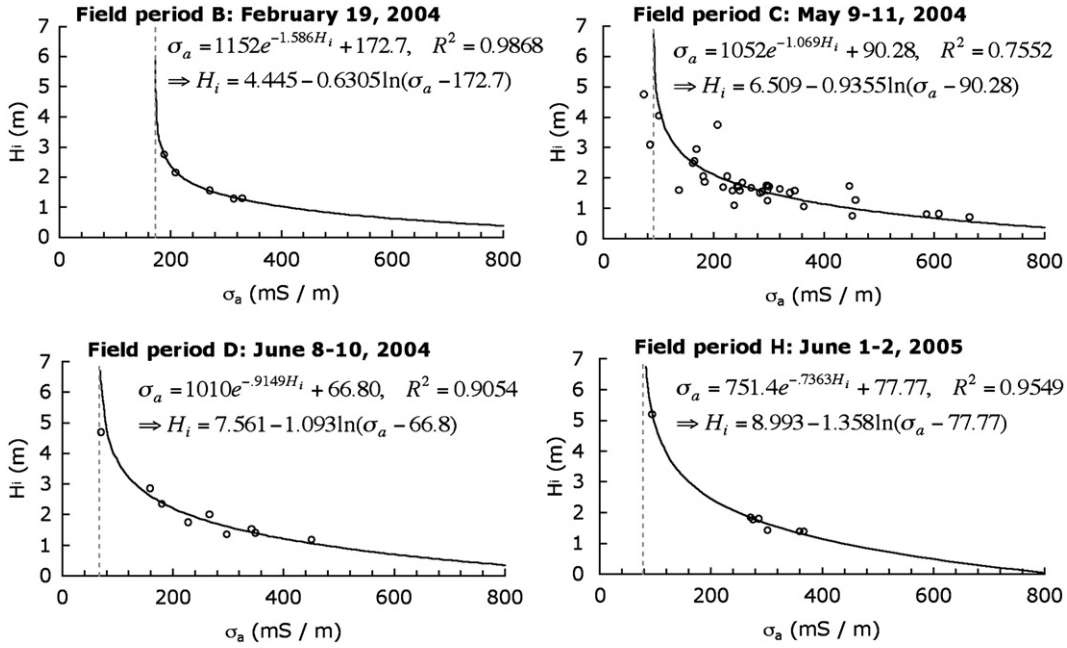

Fig. 5. Measurements of thickness and apparent conductivity of landfast sea ice for 4 different field periods. The curves show the logarithmic functions empirically derived from the measurements, which are shown by circles. The dotted lines indicate the asymptotes of the logarithms.

below the asymptotic value of the fitted curve. This demonstrates the limits of simple curve fitting when the substrate being measured consists of a complex distribution of sea ice, seawater and air. There were many other points at which measured values of σ_a were lower than the empirically derived asymptotic value. In these cases, the formulae cannot be applied to transform the conductivity measurements into ice thicknesses and instead the keel depth must be estimated from ice surface elevation. Section 4.7 discusses this in more detail.

The elevation of the ice or snow surface was measured using a differential global positioning system (DGPS) device operated in real-time kinematic (RTK) mode. The precision of such measurements is typically within a few centimeters, but differences between reference ellipsoids and local sea level are on the order of meters in this area. The surveys were therefore not tied to any reference ellipsoid but instead tied to local sea level through elevation measurements made at drill holes where the freeboard and hence elevation of the ice could be measured independently. Agreement between drill hole comparisons was within 5 cm.

Measurements of ice thickness and topography were made concurrently along 5 separate transects adopting one of two different sampling methods (see Fig. 2 for transect locations). In the first method, the EM-31 was towed by hand on a plastic sled while the DGPS receiver was carried in a backpack. Conductivity and DGPS location measurements were made at approximately 4 m and 20-m intervals respectively. The location of each conductivity measurement was interpolated between DGPS measurements. In the second sampling method, the EM-31 was housed inside a polyethylene kayak to which the DGPS was also mounted. Both instruments then recorded measurements at 5-s intervals while the kayak was hauled across the ice surface. Across smooth ice, the kayak was towed with a snowmobile at approximately 2 m s^{-1}, but through rough ice, the kayak was towed or carried by hand, keeping the kayak in contact with the ice. Consequently, the spacing between measurements was not constant, but varied according to ice terrain. The first method was used on transects 1 and 2 while the second method was adopted for transects 3, 4 and 5.

The transects were made as straight as possible, but the nature of the ice surface necessitated detours around inaccessibly rough areas. During field period H, the presence of continuous shear ridges rendered much of the landfast ice inaccessible and the transects were confined to trails cut through the ridges by whaling teams from Barrow. The routes of these trails are chosen to travel across the smoothest ice and, where necessary, ice is removed to cut through steep ridges and is placed into troughs between ridges to smooth out the trail. The effect of this on the measurements is to underestimate the elevation of ridge sails and the overall roughness of

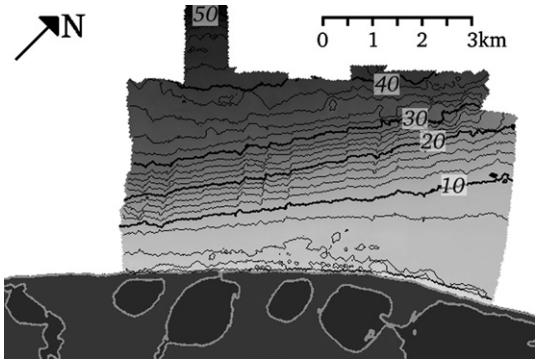

Fig. 6. The extent of the survey area and the bathymetric grid generated for this study. Isobaths are overlain in black at 2 m spacing, with bold isobaths every 10 m.

the ice surface, but the effect on the mean ice elevation is relatively small.

3.3. Sea floor pressure measurements

A Seabird SBE39 pressure gauge was deployed on the sea floor in approximately 6.5 m of water through a hole in the ice to measure changes in water depth and hence fluctuations in sea level. Fig. 2 shows the deployment location. The instrument was tethered to the ice by a 10 m long cable and data were stored onboard every minute. The instrument and data were recovered at intervals by means of drilling a slanting hole in the ice through which to hook the cable beneath the ice and retrieve the instrument. However, due to technical difficulties with the instrument, only one 45-day period of data was retrieved, which covered the time between March 31 and May 14, 2004 (Fig. 4). Although the SBE39 also records water temperature, a constant seawater density of 1027 kg m^{-3} was assumed in the calculation of water depth from the measured pressure data, which was corrected for variability in sea level atmospheric pressure.

3.4. Bathymetry survey

At the time this study was started, there were no digital high-resolution bathymetric data available covering the footprint of the land-based radar. To obtain this data, we performed a survey during field period E using a narrow-beam depth sounder mounted on a 6.5 m Lund skiff, which allowed sounding of water as shallow as 1 m. Soundings were made every 0.5 s while the boat traveled at approximately 25 m s^{-1}. The boat's location was recorded using a handheld GPS device approximately every 12 s. These datasets were then merged through averaging and linear oversampling to yield a data point every second or approximately every 25 m. A linear inverse distance interpolation was performed on these sounding points to produce a 25 m bathymetric grid (Fig. 6). After the completion of this survey, digital data became available from the National Geophysical Data Center through the Geophysical Data System (GEODAS), consisting of sounding points compiled from numerous surveys dating back to 1945. Mahoney (2006) compared these datasets and found only minor differences. For this study, we used the data from the recent survey, since it is more representative of the current seabed.

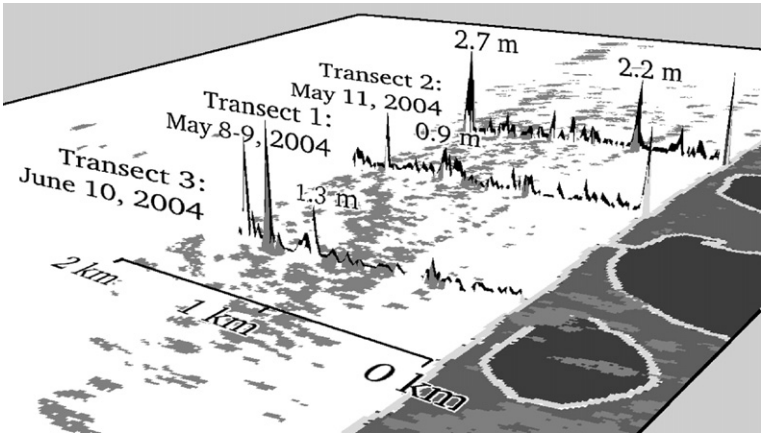

Fig. 7. The locations and dates of 3 ice elevation transects overlain on a radar image from June 10, 2004. The grey areas are targets, while the thick black lines show the elevation along each transect (note the 200× vertical exaggeration). The heights of different features along each transect are given for scale. Transects 1 and 2 show the beach slope, but transect 3 originates on the ice.

4. Results

4.1. Comparison between radar imagery and ice topography

As mentioned in Section 3.2, ice thickness and elevation transects were performed within the footprint of the radar partly for the purposes of ground-truthing the imagery. Fig. 7 shows the elevations measured along 3 transects overlain on a radar image from June 10, 2004. The transects were performed on the dates shown, during field periods C and D (Fig. 4). Fig. 7 shows that target size is not a reliable indicator of the size of topographic feature, for the reasons discussed in Section 3.1. However, it should also be noted that there is a large difference between the effective sampling sizes of the elevation transect and the radar; although a transect may pass through a target in the radar imagery, the corresponding feature of the ice surface may lie to the side of the transect. Also, the transect may pass through shadow zones, as illustrated in Fig. 3. Due to these constraints, we do not interpret features based solely on a single image. Where possible we refer to field observations or the behavior of targets in animated time-series of imagery to increase the amount of information used in this analysis.

4.2. Summary of the 2003–04 landfast ice season

The 2003–04 ice season at Barrow was notable for the late onset of landfast ice formation. No ice was visible in the field of view of the radar until November 5 and no ice attached to the coast until November 12 when floes drifting past the coast to the Southwest apparently grounded. This ice extended approximately 800 m from shore, but most of it detached again on November 21 upon interaction with pack ice drifting past to the NE. The majority of the landfast ice that remained for the rest of the year was accreted during an event beginning in the morning of November 25 when the pack ice converged on the coast from the west. Early in this process, a line of targets appeared in the imagery along the boundary between the landfast ice and pack ice. Field observations on December 10, 2003 showed some of these targets (outlined in Fig. 8a) represented a 2−4 m high ridge composed of broken ice approximately 50 cm thick. Tide cracks around the ridges suggest they were grounded.

Ice continued to converge upon the coast from the west and targets drifted toward shore and became stationary. Although the distance between targets decreased, few new targets appeared after the initial ridge building on November 25 suggesting that little ice deformation occurred and open water occupied at least part of this area. Convergence continued until approximately 9 pm on November 26, at which time a well-defined discontinuity appeared 3 km offshore along which pack ice began moving northeastwards at approximately 2–3 km/h. This discontinuity is well described as a line of slippage. Fig. 8(a) shows radar imagery from this time, with the slippage line indicated in black. Offshore of this line of slippage, pack ice drifted past northeastwards at 2–3 km/h parallel to the coast with little noticeable drag, while the shoreward ice ceased deforming and remained stationary.

On January 4, 2004, a large pack ice floe traveling northeastwards sheared off the outer edge of the landfast ice. This created a new landfast ice edge marked by a line of targets. Fig. 8(b) shows the resulting landfast ice edge, which is discussed in more detail in Section 4.4. Other than this event, however, the landfast ice formed on November 26 remained largely unchanged until sometime between February 25 and March 9, during which time the radar obtained no data (Fig. 4). The first imagery on March 9 shows no moving targets, but reveals that some of the landfast ice targets changed or are missing since February 25. The radar imagery next shows ice motion on March 19 when a large section of ice moved away from the coast. The resulting landfast ice edge (Fig. 8c) coincided with the boundary between new and pre-existing targets on March 9. This suggests that a flaw lead opened and closed along this edge while the radar was not operational and that the ice that reattached seaward of the line was not stable. The targets shoreward of the line can be recognized as those that were emplaced on November 26 (Fig. 8a).

Over the next 9 days, a complex series of accretion events extended the landfast ice width to about 5.5 km from the shore. Fig. 8(d) shows an irregular landfast ice edge that existed briefly during this period, part of which is the same as that seen on March 19 (Fig. 8c) and part of which represents the addition of a new section of landfast ice. Section 4.5 fully describes the events during this period. The resulting landfast ice extent was the maximum achieved in the 2003–04 annual cycle and remained unchanged until mid-May. The location of the landfast ice edge approached the effective range of the radar, though targets could be seen moving at this edge throughout April and into May. The next detachment occurred sometime between May 20 and 24 while the radar was not operational. The radar imagery on May 24 (Fig. 8e) shows an irregular edge that partly matches that seen on March 22 (Fig. 8d). This suggests the presence of a grounded floe or ridge near the convex section of the landfast ice edge.

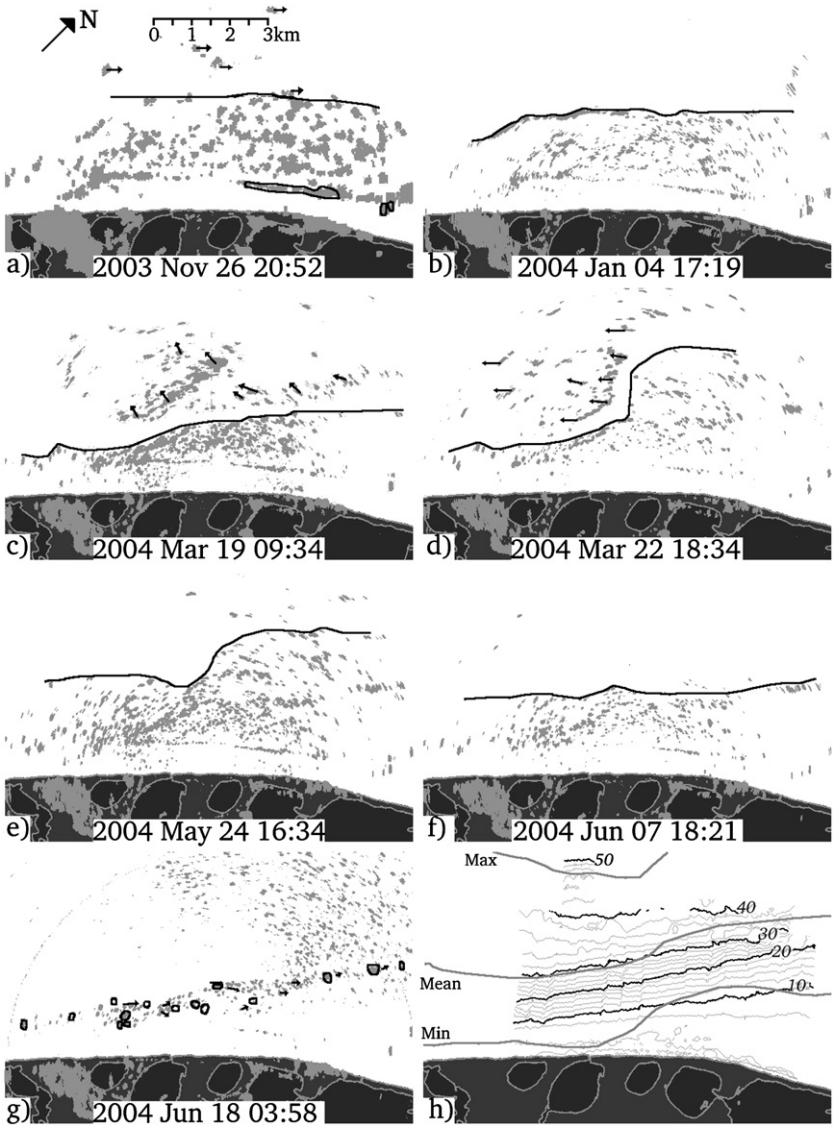

Fig. 8. (a–g) Radar images capturing key events in the evolution of the landfast ice near Barrow in the 2003–04 ice season. Outlined targets indicate grounded floes. Other lines delineate the seaward edge of the landfast ice. Black arrows indicate the motion of targets in the animated imagery. (h) The 1997–2004 minimum, mean and maximum seaward locations of the landfast ice edge for the month of March overlain on the local bathymetry. Black and grey contours are at 10 and 2-m intervals respectively.

Between May 30 and June 7, during another period without radar data, more landfast ice detached leaving a straighter landfast ice edge intersecting points along previous locations of the landfast ice edge parallel to the shore (Fig. 8f). The final break-up of the landfast ice began on June 16 when pack ice floes drifted rapidly past the landfast ice. The animated imagery shows drifting targets eroding the landfast ice edge and leaving isolated stationary targets amidst moving targets. This is strong evidence that the remaining stationary targets represented grounded floes. The outlined targets in Fig. 8(g) show their locations.

Fig. 8(h) shows the minimum, mean and maximum seaward landfast ice edges for the month of March derived from satellite images between 1997 and 2004 (Mahoney et al., in press). The landfast ice edges derived in this study from the land-based radar lie close to the mean. Also, the shape of the satellite-derived edges indicates that sections of landfast ice to the Southwest of the radar frequently detach while the ice to the Northwest remains, as occurred on March 22 and May 24, 2004 (Fig. 8d and f). Fig. 8(h) also shows that the orientation and location of the 20 m isobath corresponds well to the

zone of grounded ridges in Fig. 8g. These grounded ridges constrained the location to which the landfast ice edge retreated during the detachment events between February 25 and March 9 and on March 19 (Fig. 8c). However, the landfast ice edge frequently occupied water deeper than that in which ice typically becomes grounded, at which times its shape may be influenced by the proximity of Point Barrow.

4.3. Summary of the 2004–05 landfast ice season

Although the radar was not operational for a significant fraction of the 2004–05 ice season, it is still possible to ascertain the nature of events that shaped the landfast ice through its annual cycle. The first accretion of landfast ice took place earlier than in the previous year and in a more complex fashion. The first ice came into view of the radar on October 11, drifting northeastwards past the coast. Stationary targets approximately 200 m from the shore (corresponding to 2–4 m water depth) on October 29 were the first evidence of landfast ice in this annual cycle. Beyond these, pack ice targets traveled southwestwards at about 3 km/h.

Over the next 2 weeks, pack ice continued moving past the coast reversing direction 6 times. During this period, the landfast ice extended to just over 1 km in width during a series of accretion, slippage and detachment events. As the pack ice drifted past the radar, the outlines of individual floes could be identified in the imagery. Many of the floes rotated as their shoreward edges dragged past the landfast ice edge (Fig. 9a), unlike the occurrence of slippage in November, 2003. This implies that there was shear stress at the landfast ice edge, but it also indicates only weak compressive stress between ice floes. Along with the absence of new targets being created at the time, this suggests that little ridge formation was taking place.

A brief period of continuous radar data on December 10 shows that the landfast ice advanced sometime after December 4. However, the imagery shows drifting targets moving between stationary targets (Fig. 9b), which indicate that the landfast ice was in the process of

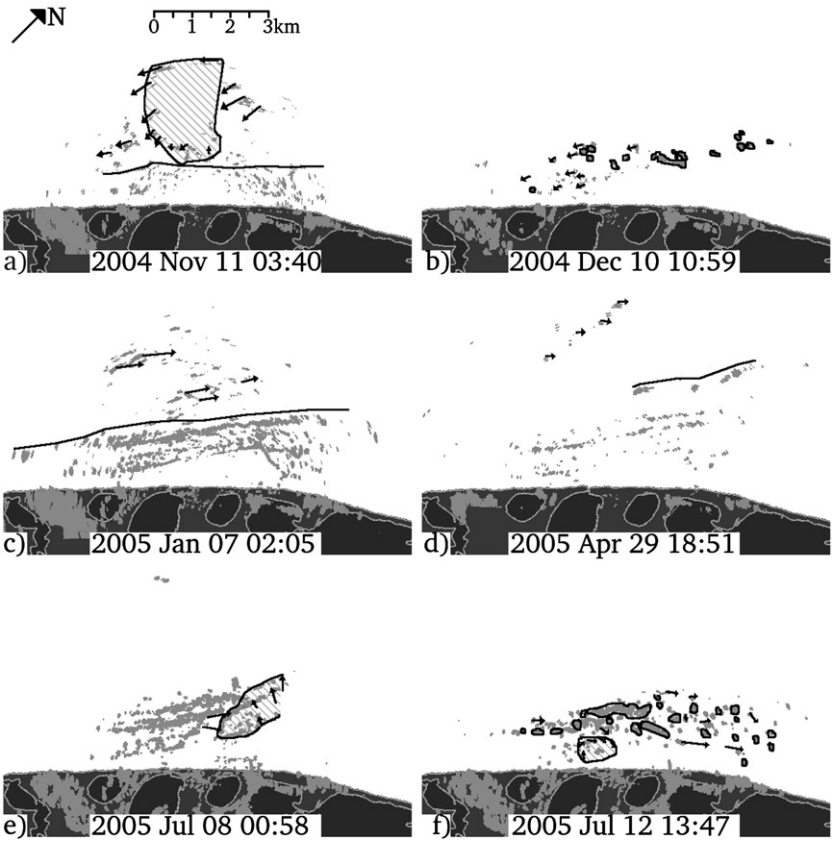

Fig. 9. Radar images capturing key events in the annual cycle of landfast ice near Barrow in the 2004–05 ice season. Outlined single targets indicate locations of grounded floes. Outlined hatched areas indicate groups of targets behaving as rigid bodies. Other lines delineate the seaward edge of the landfast ice. Arrows indicate the motion of targets in the animated imagery.

breaking up at this time. The stationary targets (outlined in Fig. 9b) are interpreted to be grounded floes and their distribution closely resembles that seen on June 18, 2004 (Fig. 8g). Fig. 9(c) is an image from another brief period of operation of the radar between January 7 and 8 that shows the landfast ice had reformed and extended in the intervening period. A significant amount of ice ridging apparently occurred during this process as the image shows 3 distinct lines of targets parallel to the isobaths (see Fig. 6 for bathymetry). Subsequent field observations (Section 4.7) showed that these targets corresponded to a broad zone of deformation containing several shear ridges. A comparison with the radar data from December 10 (Fig. 9b) shows that the zone occupied by the ridges is the same as that previously occupied by stationary targets and that only the most shoreward grounded ridges, if any, remained in place.

Although the radar did not observe the formation of these three ridges, data from April 29 captured the accretion of a fifth ridge. Fig. 9(d) shows the newly created targets just shoreward of the landfast ice edge. Although no observed targets converged directly on the landfast ice during this episode (probably due to shadowing from the ridges nearer shore; see Fig. 3), targets were drifting northeastwards, obliquely towards the landfast ice edge, as the line of targets appeared representing the fifth ridge. The manner in which this ridge was formed suggests that each of the other ridges may have been emplaced in its own separate event. Their orientation parallel to the local isobaths suggests that they were emplaced under similar northeastward drift.

Although subsequent radar imagery is not continuous, no further change was seen until July 8 when a large section of landfast ice broke away as a single unit. The radar image in Fig. 9e, captured shortly after detachment, shows that the landfast ice broke along a line intersecting the main ridges. This suggests that these ridges were not continuously grounded and that long sections may have been floating freely. It also demonstrates that break-up is not simply the reversal of formation. Over the next 5 days, the remaining landfast ice broke-up in sections, often drifting and becoming stationary again within the view of the radar. Fig. 9f shows briefly grounded floes amidst drifting and rotating floes on July 12. For several more days, targets continued to drift in front of the radar, many of which also exhibited motion indicative of gouging, and it is not until sometime between July 15 and July 17 that the coast was completely free of ice. Therefore not only was this break-up over 3 weeks later than the previous year, but the manner of break-up was also markedly different. These differences are probably related and are discussed in Section 5.

4.4. The "freight train" event, January 4, 2004

Fig. 10 shows a sequence of radar images acquired 20 min apart on January 4, 2004 that capture the deformation of landfast ice caused by a large ice floe traveling northeastwards amongst the ice pack. Prior to this, animated imagery shows the pack ice converging and moving around a promontory of landfast ice immediately offshore from the radar (Fig. 10a). Just before 4 p.m. a large floe traveling at approximately 4 km/h struck this promontory and sheared it off from the landfast ice. Few targets were visible on the floe and so its overall size is uncertain, but ice deformation around it suggests it was at least 1.5 km across. Hatched areas in Fig. 10 show the inferred extent of the impinging floe. In addition to shearing-off the promontory to leave a landfast ice edge more aligned with the coast, the floe also caused deformation of the pack and landfast ice ahead of it, the extent of which is shown by the zig-zagged areas in Fig. 10. The areas of these damage zones indicate that the floe deformed landfast ice approximately 1 km shoreward of its path.

This event shows that the path of a single large floe can determine the position of the landfast ice edge. The impinging floe in this case maintained a constant trajectory and was not deflected as it deformed the landfast ice, which therefore was most likely not grounded. The resulting landfast ice edge, which marks the path of the shoreward edge of the floe, intersects local isobaths obliquely and enters water shallower than 20 m before it leaves the radar's field of view. This suggests that the shoreward edge of the floe did not contain any keels deeper than 20 m and that the path of the floe was constrained by the large scale shape of the coast and not local bathymetry.

4.5. The "compactor" event, March 19–25, 2004

A detachment event on March 19 (Section 4.2 and Fig. 8c) was the first of a series of events during which the landfast ice underwent significant change. After moving away from the coast to the west, the pack ice reversed direction approximately 12 h later so that some targets remained in the radar's field of view and met the landfast ice approximately 4 km from where they had detached. Pack ice continued to converge and deform for another 2 days before pulling away from the coast to the west once more on March 22, leaving a new landfast ice edge. Fig. 8d shows this event. A particularly notable feature of the animated radar data of both these detachments is the flickering of targets that move, prior to their movement. This flickering is discussed in more detail in Section 4.6.

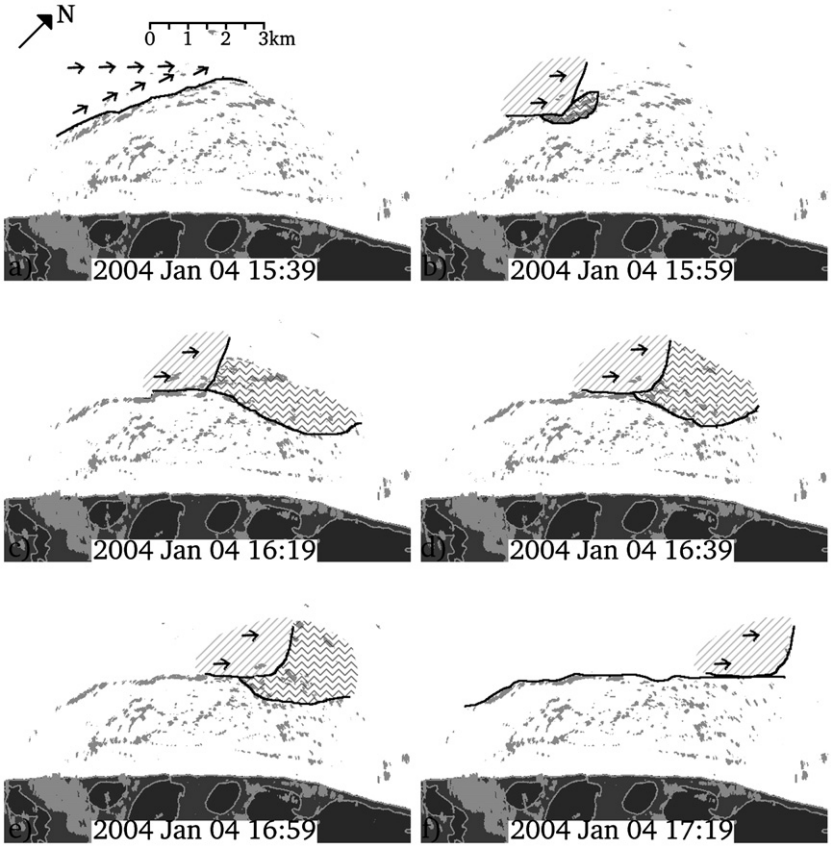

Fig. 10. Deformation of landfast ice on January 4, 2004 caused by a large floe traveling northeastwards along the coast. The arrows indicate the sense of ice motion seen in the animated imagery and the black lines in a) and f) show the landfast sea ice edge. The hatched area indicates the inferred extent of the impinging ice floe. The zig-zagged areas show the extent of the damage zone ahead of the floe. The reader is strongly encouraged to view the animated imagery referred to in the text.

Following the second of these two detachments, pack ice drifted past the radar to the Southwest. The shape of the visible landfast ice edge at this time created an area in the lee of pack ice motion, which remained free of targets for nearly 2 days before the pack ice again drifted shoreward. The deformation pattern of the ice pack as it did so reveals that the target-free area actually contained level ice, as would be expected after 48 h with a mean air temperature of −25 °C. A simple freezing degree day model (Maykut, 1986) predicts 20 cm of ice growth starting from open water during this time, which agrees with field observations of the block size of ridges in this area in June, 2004.

Fig. 11 shows a series of 6 radar images capturing the closure of this newly-refrozen lead (shown by the zig-zagged hatching) over the following 12 h. The animated imagery captures this dynamic event in remarkable detail and we encourage the reader to view the animations, which are available from website given in Section 3.1 or on DVD from the authors upon request. Initially, the level ice remained intact and pack ice targets came to rest briefly at the seaward edge of the target-free area (Fig. 11b). The subsequent failure and ridging of the level ice was not a continuous process but occurred in episodes, the longest of which lasted about 1 h and resulted in approximately 700 m of shoreward motion. In addition, motion was not uniform along the advancing pack ice edge. Instead, the level ice demonstrated non-simultaneous failure (Kovacs and Sodhi, 1988), resulting in the irregular shape of the target-free (zig-zagged) area as the refrozen lead closed.

4.6. Flickering of radar targets

We adopt the term “flickering” from Shapiro (1987) to describe the alternating appearance and disappearance of targets within a region of radar imagery, without any apparent movement of the targets. Typically, the disappearance of one target coincides with the appearance of another target nearby, such that the overall number of

targets remains fairly constant. The sampling rate of the radar imagery (Section 3.1) prohibited a detailed frequency analysis, but no periodicity was apparent in the appearances and disappearances of targets. Flickering only affects sea ice targets and can be limited to distinct regions of landfast ice. In the animated imagery, stationary targets also exhibit fluctuations in size over time, which are thought to be largely related to temperature sensitivity of the antenna (Mahoney, 2006). This is a phenomenon distinct from flickering however and is not observed by the technique described below.

Flickering was first observed in radar data obtained near Barrow in the 1970s (Shapiro, 1987) in conjunction with bottom pressure data that showed sea level fluctuations of approx 1 cm amplitude and 6–10-min period (Shapiro, pers. comm.). This suggests that flickering represents vibration or small-scale motion of the ice in response to the passage of waves through the water. This would lead to changes in local grazing angle of the radar energy and therefore fluctuation of backscatter (Section 3.1). Shapiro (pers. comm., 2006) noted that flickering often preceded ice motion. Although not every flickering event preceded motion, neither the pack or landfast ice was observed to move without flickering beforehand.

Flickering was observed on a number of occasions in this study. By calculating the net difference between three consecutive images after assigning values of 1 and 0 to target and non-target pixels respectively, we created series of "flicker images". In these, values greater than zero indicate pixels that have appeared and/or disappeared during the 3-image sequence. In most flicker images, non-zero pixel values only occur around the peripheries of targets due to small changes in target size. However, during true flickering, entire targets exhibit non-zero pixel values in a flicker image. Although this still leaves a degree of subjectivity to the identification of flickering events, it makes determination of the onset

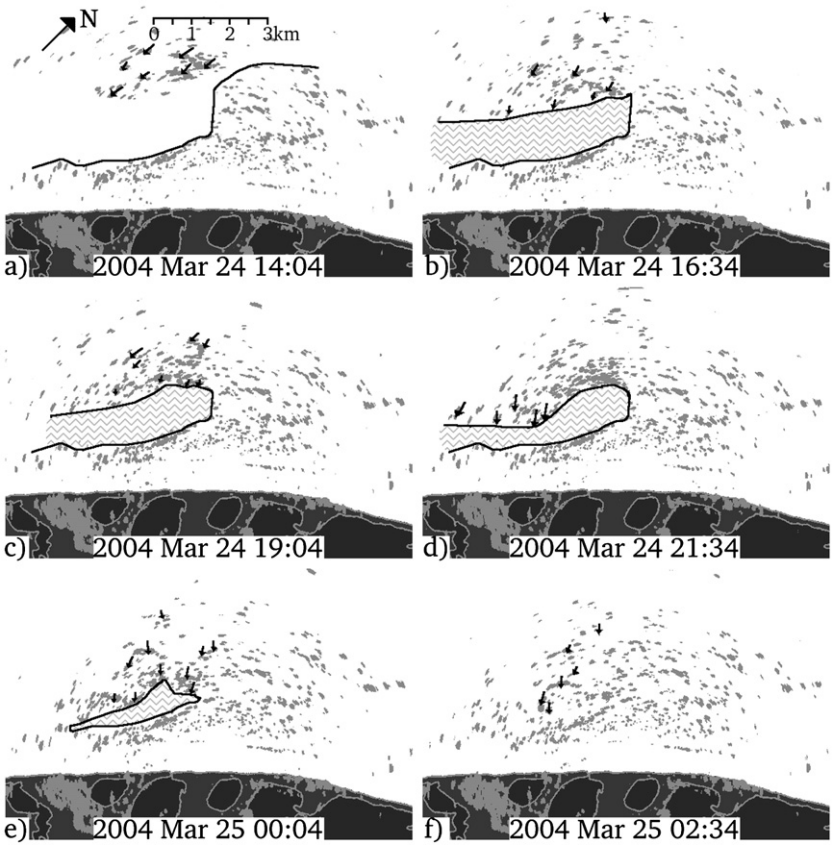

Fig. 11. Closure of a refrozen lead inferred from animated radar imagery, field observations and an ice growth model. The orange line in (a) indicates the location of the landfast ice edge following a detachment event on March 22 (also shown in Fig. 8d). The zig-zagged area indicates the inferred extent of the level ice. Arrows show the motion of targets derived from animated imagery. We encourage the reader to view the animated imagery referred to in the text.

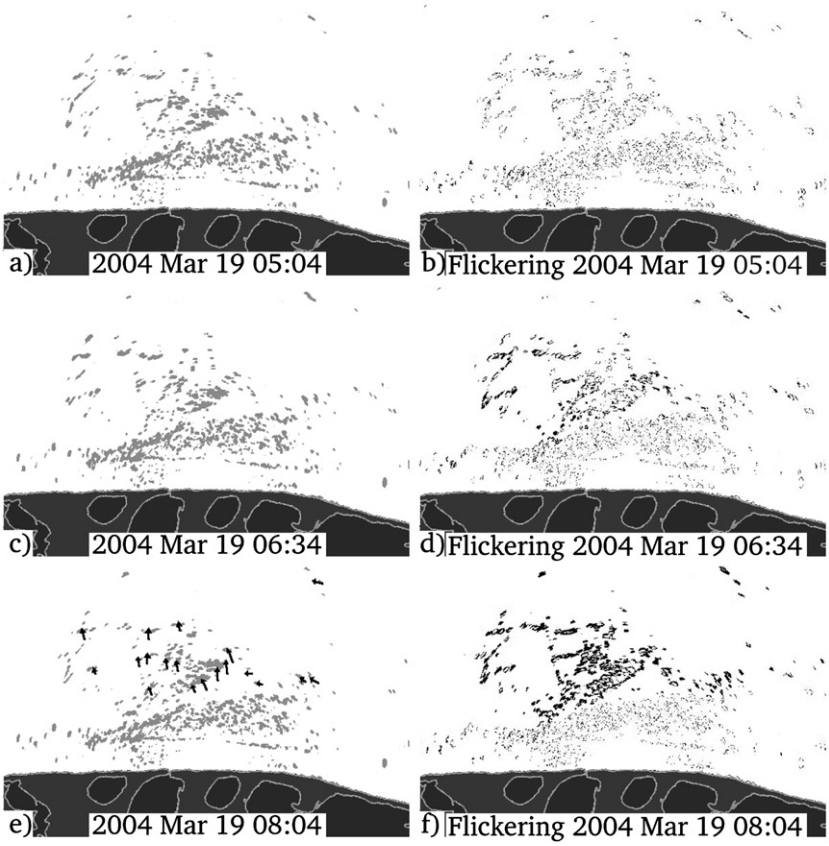

Fig. 12. Flickering of targets prior to ice motion. (a,c,e) 3 Radar images capturing the detachment event on March 19, 2004 and (b,d,f) their corresponding flicker images showing that flickering only affected those targets that moved and was apparent up to 30 min prior to ice motion. Black arrows in (e) indicate the net motion of targets by 08:04 AST.

of the phenomenon less subjective than just using original radar animations.

Fig. 12 shows 3 radar images taken 90 min apart with the corresponding flicker images. Each flicker image was calculated from the 3 consecutive images up to and including the time indicated. These radar and flicker images cover the time before and just after the detachment event on March 19, 2004 discussed in Sections 4.2 and 4.5. The first detectable ice motion occurred at 07:04 AST. Fig. 12(b) shows the flicker image 2 h prior to this motion, when only the peripheral pixels of targets show any change. The first observation of flickering occurs in the flicker image corresponding to 06:34 AST (Fig. 12d), in which larger black features indicate whole targets that are appearing or disappearing. Animated flicker images (available at the website given in Section 3.1 or on DVD from the authors upon request) show that the degree of flickering increases until the first ice motion is observed, at which time it becomes clear that flickering affected only those targets that subsequently moved. Fig. 12(e) indicates the amount of ice motion that occurred in 1 h. It should be noted that the black targets in Fig. 12(f) are partly due to ice motion rather than flickering, but the degree of flickering detected is representative of that immediately prior to ice motion.

Flickering also occurred several hours prior to the detachment event that followed soon after on March 22 (Sections 4.2 and 4.5), though the degree of flickering fluctuated during this time. Flickering was also evident several days before the onset of final break-up of the landfast ice in June, 2004 and several hours before the ice motion early on July 8, 2005. The large landfast section that broke away on this latter date (Fig. 9e) showed the most intense flickering about 3 h prior to motion.

Shapiro (1987) also noted occurrences of flickering not followed by ice motion. Although flicker images were not produced for every radar image acquired during our study period, no other obvious flickering events were noted other than those mentioned above, all

of which were followed by ice motion. Flicker images were produced from all the imagery available during the operation of the seafloor pressure gauge (Fig. 4). During this period, there was a single brief instance of flickering on May 13 that affected the line of targets nearest shore (Fig. 8a), which is not noticeable in the original animated imagery. This event is discussed in the context of the other features of the bottom pressure record in Section 4.8. No other targets exhibited flickering and the event lasted just 40 min, but it suggests that there could have been other subtle flickering events that went undetected.

4.7. Locations of grounded floes and ridges

Lacking direct observations from beneath the ice, we must infer from surface evidence whether or not landfast ice is floating. For example, the locations of grounded landfast ice can be inferred from stationary targets amidst moving targets in the radar imagery (Sections 4.2 and 4.3). Also, the observation of a tide crack around a large floe or ridge suggests that the ice rests upon the seabed (Section 4.2). In theory, combining measurements of ice surface elevation, ice thickness and water depth can also identify the locations of grounded features.

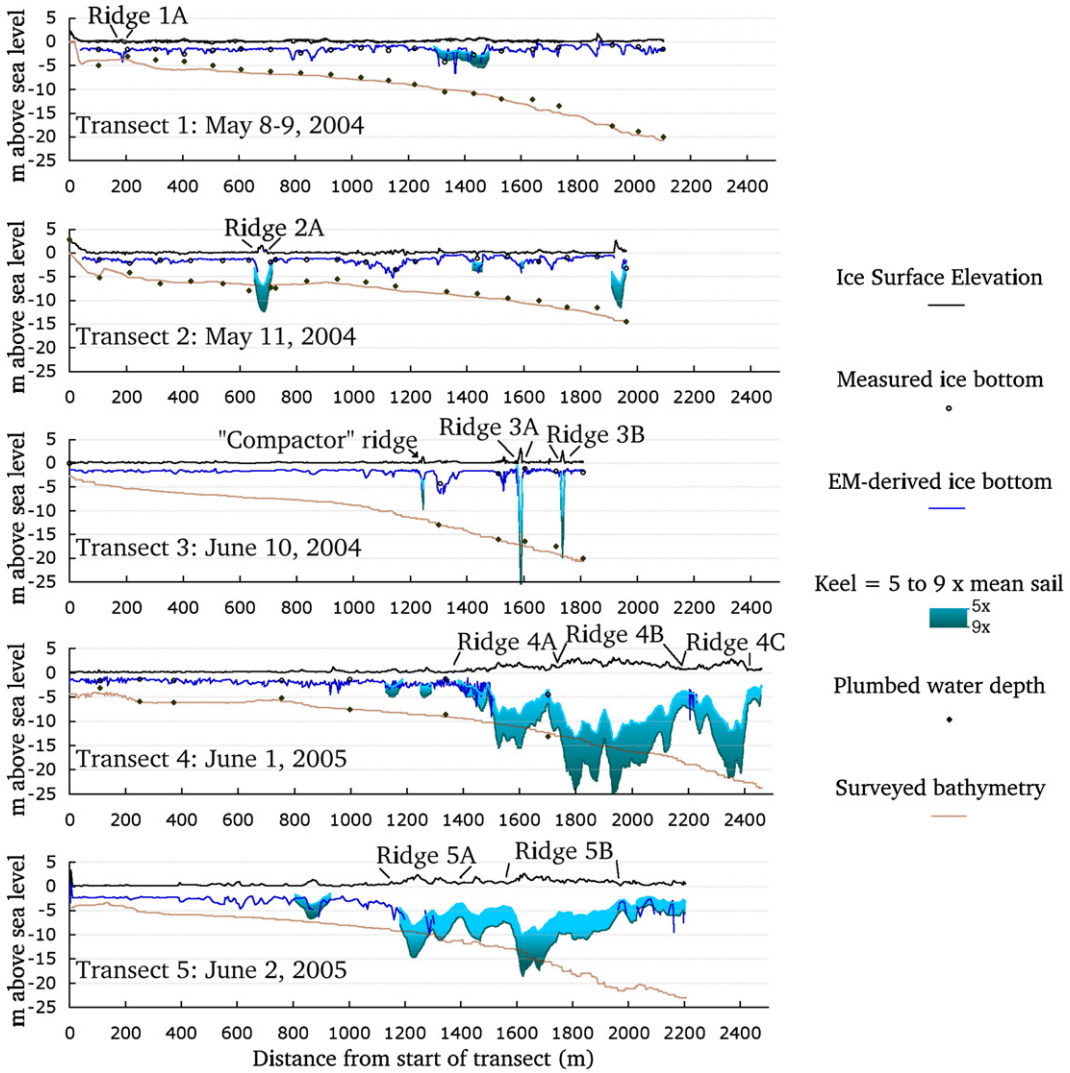

Fig. 13. Surface and bottom topography of sea ice combined with bathymetry to identify grounded ridges. Ice thickness is derived from drilling, EM measurements (Section 3.2) and keel height to mean sail height ratios (H_k/H_s) of 5 and 9. Bathymetry is derived from plumbline measurements and the interpolated bathymetric grid (Section 3.4). Each transect started on or within 100 m of the beach (see Fig. 2 for locations).

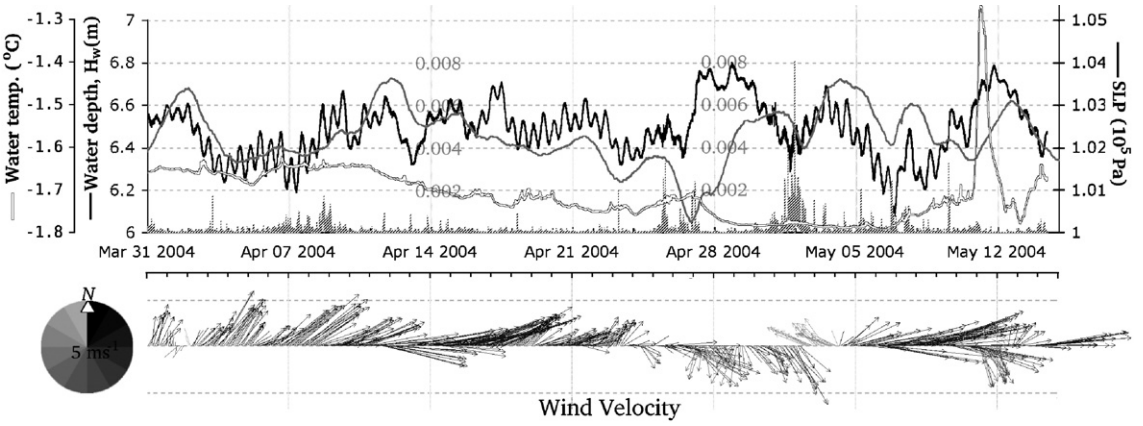

Fig. 14. Variation in water depth (black curve) and water temperature (white curve with black outline) recorded by a sea floor pressure gauge deployed beneath the ice between March 31 and May 14, 2004. The hatched bars at the bottom of the plot show the variance in sea level over 10-min intervals (grey labels on the horizontal gridlines indicate magnitude). The grey curve shows the variation in sea level pressure (SLP). The vectors show wind velocity, pointing upwind.

Fig. 13 combines the data from 5 ice thickness and topography transects (Section 3.2) with results from the bathymetry survey (Section 3.4). Fig. 2 shows the locations of all transects. The difficulty with this approach is an accurate determination of the thickness of ice that is sufficiently thick to reach the seabed. As discussed in Section 3.2, the empirically derived relationships between apparent conductivity and ice thickness break down over thick, deformed ice. This is responsible for the discontinuous nature of the EM-derived ice bottom curves in Fig. 13. In these transect sections, we must instead estimate the thickness of the keel based on a ratio of keel height to sail draft, H_k/H_s.

The calculated grounded length of each transect depends upon the value of H_k/H_s, which is determined by the geometry, porosity and ice density of the sail and keel. Timco and Burden (1997) give a mean value of H_k/H_s of 4.5, with a standard deviation of 1.9, noting little difference between ridges in the Beaufort Sea and ridges in other, temperate seas. For the Baltic Sea, Leppäranta and Hakala (1992) calculated a mean value of 5.5, with a standard deviation of 2.5 and observed that larger ridges appear to have a larger value of H_k/H_s. In Fig. 13, the ice bottom is estimated using the mean sail height over a distance of approximately 40 m and values of H_k/H_s of between 5 and 9. A value of 5 was the smallest ratio indicating any grounded ice along the transects, while a ratio of 9 corresponds to the proverbial iceberg with equal width, porosity and ice density in both the sail and keel.

Fig. 13 shows a striking difference in the number and size of grounded floes between 2004 and 2005. Based on the surveyed bathymetry, the 3 transects measured in 2004 indicate only 4 small possibly grounded ridges. These are labeled alphabetically for each transect in Fig. 13. This figure also shows the ridge formed as a result of the "compactor" event on March 25, 2004 (Section 4.5), when a refrozen lead at the landfast ice edge was deformed by pack ice (Fig. 11). Although radar imagery in June 2004 showed grounded features in this area, the "compactor" ridge does not appear to be grounded where it was crossed by transect 3.

Summing the distances over which keels intersect the seabed and dividing by the combined lengths of transects 1, 2 and 3 yields fractional grounded lengths of between 1% and 2% for values H_k/H_s between 5 and 9. The ridges observed in 2004 varied in height along their axes. Also, none of the grounded ridges observed in the 2004 transects lay within the zone of grounded features identified in the radar imagery during break-up in June (Fig. 8g), suggesting that the landfast ice was anchored by small and discontinuous ridges. By contrast, data from 2005 identified 5 separate grounded features in a broad, continuous area of deformed ice. Along transects 4 and 5, the combined fractional grounded length was between 1% and 12% for values of H_k/H_s between 5 and 9. Furthermore, <8% of the grounded landfast ice in 2004 lay in water deeper than 10 m, while >80% did so in 2005. Section 5 discusses the anchoring strength provided to the landfast ice by these ridges.

4.8. Sea level variability

The black curve in Fig. 14 shows the water depth, H_w, calculated at the location indicated in Fig. 2 from sea floor pressure measurements between March 31 and May 14, 2004 (Section 3.3). The mean water depth over the period was 6.5 m. Fig. 14 shows semi-diurnal tides with amplitudes of about 5 cm, as well as longer-

timescale variability that was considerably larger. The overall range of sea level during the observation period was 73 cm. The grey curve shows sea level pressure (SLP) measured at Barrow Post–Rogers Airport. It is plotted at a scale such that 100 Pa of SLP is equivalent to a 1 cm of H_w, which is approximately the magnitude of the inverse barometer effect. Although the magnitudes of the variability in H_w and SLP compare well, sea level did not respond to local SLP in a simple inverse fashion. This is expected near the coast where wind typically drives changes in sea level, but the local wind data for the time period, plotted at the bottom of Fig. 14, also show no simple relationship to measured sea level.

Fourier analyses showed a distinct peak in the power spectrum of H_w at 12.1 h, corresponding to the semi-diurnal tide. The spectra of H_w, SLP and different components of wind velocity were similar for time periods of between 1 and 5 days indicating that they all varied at similar timescales. Cross-correlation analyses, performed over running 5-day subsets between H_w and SLP and the wind data, indicate a complex relationship between the atmosphere and local sea level. At the beginning of the study period, there is a strong positive relationship between H_w and SLP ($r>0.8$) at a lag of between 6 and 12 h, opposite to the effect predicted by the inverse barometer effect. Over time, the value and lag of the peak correlation changes magnitude and sign. The onshore and alongshore components of wind exhibit similarly variable correlation peaks and lags. This result is surprising, given the good correspondence between surface wind and current measurements observed at a mooring beneath pack ice in the Chukchi Sea near Wainwright (Weingartner, pers. comm., 2006). It is not clear whether the landfast ice is responsible for modulating the atmospherically driven sea level variation or whether the abrupt change in coastal aspect at nearby Point Barrow complicates the under-ice regime. This suggests that modification of coastal surges is another possible important role of landfast ice in the nearshore environment. Unfortunately, it also prevents us from obtaining a simple relationship such as the inverse barometer effect allowing us to infer changes in sea level during the periods lacking sea floor pressure data.

Fig. 14 also shows higher frequency sea level variability. The grey bars below the water depth and SLP curves show the variance in water depth over 10-min intervals. Grey labels on the horizontal gridlines show the magnitude of the variance. These show that during the 45-day measurement period, there were a number of episodes during which sea floor pressure fluctuated by the equivalent of several cm of water over time periods of minutes. These episodes varied in their intensity and duration and do not correspond uniquely to any atmospheric variability. The 2 strongest episodes, between April 25–27 and April 30–May 2, coincided with offshore (southeasterly) winds, but an earlier prolonged episode, April 6–8, did not. In addition, there were southeasterly winds on May 11 not associated with high-frequency fluctuations in sea floor pressure.

Aoki et al. (2000) observed high-frequency oscillations of sea level of similar magnitude using GPS and video equipment mounted on floating Antarctic sea ice. However, the measurements in this study represent fluctuations in water pressure, which only correspond to changes in sea level under hydrostatic conditions. These high-frequency episodes may therefore indicate the occurrence of strong currents or turbulence beneath the ice. Marsden et al. (1994) suggested that internal waves caused by the interaction between tidal currents and ridge keels could be responsible for high-frequency variations in vertical current velocity observed beneath landfast ice in the Canadian Archipelago. The pressure gauge was anchored at one end by around 4 kg of metal attached by approximately 10 cm of cable. Movement of the gauge on the seabed may therefore have contributed to the high-frequency variability, but this would presumably have required a significant current at the seabed.

Bates and Shapiro (1980) observed fluctuations in sea level beneath landfast ice near Barrow of several centimeters amplitude and around 600 s period. On one occasion, these were associated with increased compressive stress recorded by stress transducers in the ice. Bates and Shapiro postulated that this represented the response of ice to long-period gravity waves. Detailed Fourier analyses of running 4-hour subsets of the data in this study showed no consistent peaks in the power spectra during these episodes, suggesting that these rapid fluctuations were largely aperiodic, except for a few hours on May 1, during the peak of the second episode, when there was a well-defined peak in the power spectrum at around 23 min.

5. Discussion

In Section 4.7, up to 9 grounded ridges were identified in all 5 transects, depending on the value chosen for H_k/H_s. Using these data and equations discussed in Section 1 we now examine how well attached the landfast ice near Barrow was in 2004 and 2005. We start by considering each grounded ridge and, for simplicity, assuming that a tide crack exists around it so that it is decoupled form the surrounding level ice. We then treat the interaction of the keel with the seabed in two ways and calculate the anchoring strength provided by the grounded ridge in each case.

First, we assume no gouging; such as might occur through in situ ridging or by the keel shearing-off as it entered shallow water. From the transect data, we calculate the cross-sectional area of the ridge. Using a sail porosity of 19% (Leppäranta and Hakala, 1992) we then calculate the keel porosity that would result in buoyancy for an ungrounded ridge for a given value of H_k/H_s, using Archimedes' Law. In doing this, we assume equal sea ice density in the sail and keel of 900 kg m^{-3} and a seawater density of 1000 kg m^{-3}. We then truncate the keel where it intersects the sea floor and use Archimedes' Law again to obtain the net grounded weight of the ridge, W_g. Using Eq. (1) and the keel's grounded length, l_g, we estimate the anchoring force (per unit length of ridge perpendicular to the external force) provided by friction between the ice and the seabed:

$$F_f = \sigma_{sb} l_g \tag{4}$$

The second form of seabed interaction involves gouging. We estimate the gouge depth, h_g, from the profiles in Fig. 13 without truncating the keels. Using h_g and Eq. (2), we estimate the re-gouging force (per unit length of ridge), F_g, required to move a ridge out of its gouge. This re-gouging force will impose a shear stress, σ_g, within the keel where it intersects the seabed which is given by:

$$\sigma_g = \frac{F_g}{l_g} \tag{5}$$

By assuming a keel shear strength of 14.1 kPa (Croasdale et al., 2001), we limit the gouging action of the keel and calculate typical gouge depths of between 1 and 2 m, which agree with side scan sonar observations near Barrow by Shapiro and Barnes (1991). The anchoring strength of the ridge is determined using Eq. (2) and these shear strength-limited gouge depths.

In order to compare the landfast ice observed in 2004 with that of 2005, we express the overall anchoring strength provided by all the grounded ridges as an effective shear strength by dividing the total anchoring force by the combined length of each year's transects. In doing this, we assume that the distribution of grounded ridges observed along all the transects for each year is representative of the distribution throughout the whole ice cover. Fig. 15 shows anchoring strength versus H_k/H_s for pure friction and gouging for each year. To demonstrate the sensitivity of each type of seabed coupling, separate curves show the anchoring strength for different increases in sea level.

Our calculations suggest that the grounded ridges in 2005 provided an order of magnitude greater anchoring strength than those in 2004. Also, gouging provides significantly better attachment to the coast than frictional coupling, both in terms of overall anchoring strength and in ability to withstand changes in sea level. The solid curves in Fig. 15 indicate that with no gouging, the rise in sea level required to decouple the landfast ice from the seabed would have been <10 cm in 2004 and <35 cm in 2005, even if the keel drafts were 9 times the respective sail heights. This is of lesser magnitude than fluctuations observed by the seafloor pressure gauge (Fig. 14), and so it seems unlikely that

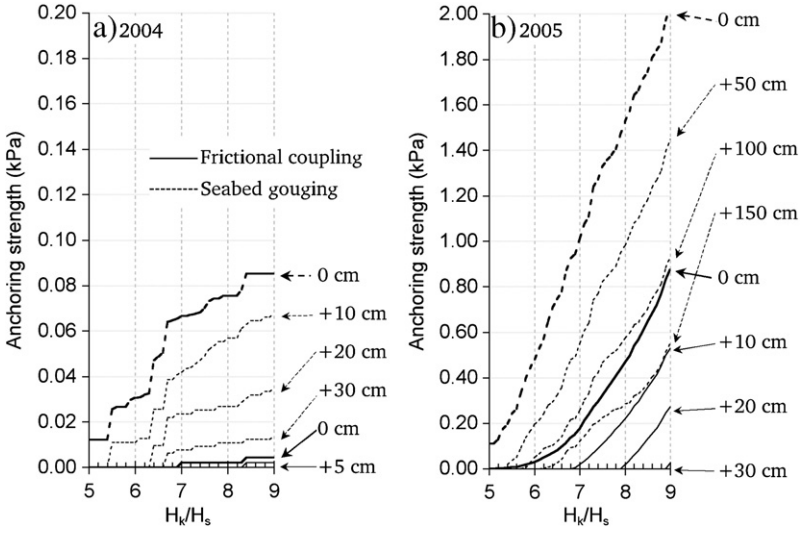

Fig. 15. The calculated anchoring strengths versus keel draft to sail height ratio provided by pure friction (solid lines) and gouging (dashed lines) for grounded ridges in a) 2004 and b) 2005. The reductions in anchoring strength for different sea levels appear in separate curves.

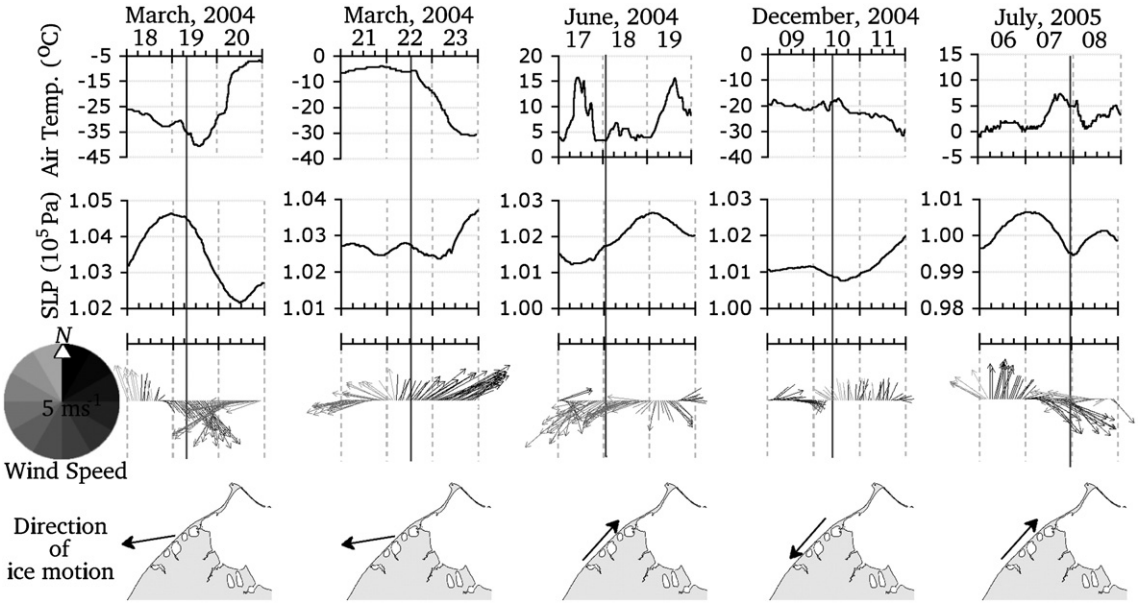

Fig. 16. Atmospheric conditions a day before and after the dates of 5 detachment events captured in the radar imagery. Note the different *y*-axis scales on each plot. Wind velocity is shown with the vectors pointing upwind. The vertical gray lines show the times that motion of landfast ice was first observed.

non-gouging grounded ridges play a significant role in anchoring the landfast ice.

The dashed curves in Fig. 15 show that the anchoring strength of gouging ridges is less sensitive to changes in sea level, but that a sea level rise of just 40 cm would have decoupled the landfast ice in 2004, even if a rather high value is taken for H_k/H_s. Given this value of 40 cm, it is perhaps surprising that the landfast ice in 2004 remained attached as long as it did, suggesting that either the bathymetry survey overestimated the water depth or the transects underestimated the number and size of grounded ridges in 2004. However, Fig. 13 shows generally good agreement between the survey data and plumbline measurements, with no particular bias toward over- or underestimating the water depths beneath grounded ridges. We are also reasonably confident that transects 1, 2 and 3 adequately sampled the landfast ice within approximately 2 km of shore. We note that we neglected to include the snow cover present in May 2004 along transects 1 and 2. However, the mean snow depth on ridge 1A was 16 cm, while on ridge 2A there was an average of 50 cm of snow. Assuming a wind-packed snow density of 300 kg m^{-3}, this would compensate for a sea level rise of 5 cm on ridge 1A and 15 cm on ridge 2A; still leaving the landfast ice significantly less well-anchored than in 2005.

Another possibility is that the ridges were more firmly grounded earlier in the year, but were only tenuously anchored at the time of measurement in spring. In particular, this could be the case for ridges 3A and 3B, which were measured on June 10 and broke away just 8 days later. Leppäranta et al. (1995) describe melting and repacking of keel blocks in spring that leads to an overall reduction in keel volume. For a grounded ridge any loss of keel draft results in an equivalent reduction in sail height until the ice floats. Also, no snow was observed along transect 3, which suggests that surface melting may have already begun by this time. Perovich et al. (2003) observed peak surface melt rates of 2.5 cm day^{-1} and bottom melt rates of 1.2 cm day^{-1} on pack ice in the Beaufort Sea in spring and summer, which would amount to a destabilizing effect equivalent to a 3 cm rise in sea level per day. This effect would be increased if the water from surface melt refroze in the keel, as suggested by Weeks (1985) for multi-year ice ridges.

Having begun to consider the conditions leading to instability of grounded ridges, we will now return to the five detachment events observed by the radar (Sections 4.2, 4.3 and 4.5). Evidence exists of other detachments during periods with no radar imagery, but the dates cannot be well defined. Knowing the precise times and dates of ice motion allows us to examine local meteorological data before, during and after such events. Fig. 16 shows the time of each of the detachment events together with air temperature, sea level pressure and wind velocity measured at Barrow Wiley Post–Will Rogers Airport along with the direction of ice motion. The events share little in common in terms of atmospheric forcing

implying local meteorological data are of little use in predicting these events. This is unsurprising, given the anchoring strength calculations above, which show that even the most tenuous frictional coupling in 2004 was comparable to the wind stress imparted by a 20 ms^{-1} wind over rough sea ice. We note here that, when directed onshore across consolidated pack ice, wind stress can be integrated over larger distances and cause shoreward movement (Mahoney et al., 2004).

Although we have no under-ice measurements, the acceleration of ice floes, at odds with wind velocity, testifies to the existence currents beneath the ice and allows us to estimate their strength. Following different detachment events, we observed ice motion of several targets that moved between 150 m and 400 m in the first hour. Since we know these targets were initially at rest, this indicates linear accelerations of $2–6\times10^{-5}$ m s^{-2}, corresponding to water stresses of 0.04–0.10 Pa, for 2 m average ice thickness. Assuming quadratic drag and taking a drag coefficient for rough landfast ice of 7.3×10^{-3} (Shirasawa, 1986), this corresponds to currents 1 m below the ice of between 7 and 12 cm s^{-1}. Currents of this magnitude are not exceptional beneath landfast ice (Langleben, 1982; Shirasawa, 1986) and the stress imparted to the ice is several orders of magnitude less than the anchoring strengths estimated above. Therefore, although such currents are likely to be the cause of ice motion away from the coast, they do not account for the decoupling that allowed the landfast ice to move.

The calculation above does not explicitly account for form drag from keels. However, there is probably no simple way in which to represent this due to the likely effect keels have on under-ice currents in such shallow waters. For example, in the presence of shallow water and continuous, deep-keeled ridges, such as in 2004–05, under-ice currents are likely to be channelized. This reduces the cross-sectional area of the keels relative to the current and the bottom surface area of the ice where skin drag occurs. With fewer, more discontinuous ridges, as in 2003–04, currents will not be as channelized and the keels will present greater cross-sections relative to different current directions. Thus, modification of under-ice currents by ridge keels may be an additional factor determining the stability of landfast sea ice.

As shown in Fig. 15, anchoring strength is sensitive to changes in sea level and so a rise in sea level may be associated with the ocean currents during detachments. Unfortunately, no bottom pressure data were available for any of the detachment events. Also, according to our calculations, the ridges in 2005 would have remained firmly attached even with a sea level rise of much greater magnitude than anything observed by the bottom pressure gauge. In this case, with detachment coming much later in the year, it seems likely that structural weakening of the ridge keels, perhaps through thermal erosion, was responsible reducing the anchoring strength of the landfast ice.

Mahoney et al. (in press) showed that in the annual cycles between 1996 and 2004, the timing of break-up of landfast ice along the northern Alaska coast correlates strongly with the onset of thawing daily mean air temperatures. This indicates that melting plays a significant role in destabilizing the landfast ice. Also, break-up was observed earlier along coasts with recurring springtime polynyas than along coasts without. This provides grounds for speculation that solar energy absorbed by the open water transfers to the landfast ice, promoting break-up. The temperature sensor on board the bottom pressure gauge recorded a pulse of warm water with temperatures above −1.3 °C lasting approximately 24 h on May 11 (Fig. 14). Moderate resolution imaging spectrometer (MODIS) imagery shows that a polynya existed adjacent to the landfast ice at Barrow under mostly clear skies for much of April and May, including the time of the warming event on May 11. The high water temperatures occurred during one of the most prolonged and rapid rises in sea level observed, suggesting an influx of warm water beneath the landfast ice. However, we note that warm water pulses were not observed during other sea level rises.

Similar pulses of warm water have been recorded beneath landfast ice by thermistor strings frozen into the ice (Cole et al., 2004). While no data are available for 2004 and 2005, data collected throughout the ice growth season of 1999 through 2001 showed a total of seven strong (0.1 to 0.8 K) warming/melt events of typically one day duration, with five of these occurring between March 28 and May 1 and the other two on November 19/20 and December 29 (Eicken et al., unpublished data). Timing of these events corresponds well with the timing of break-out events shown in Fig. 16 (though in different years). While no data on bottom melt during these episodes are available, several centimeters of melt per day under level ice have been observed in winter drifting ice (Perovich et al., 2003). It is likely that cumulative melt in a ridge keel may well exceed such rates by a factor of 2 to 5 due to greater surface to volume ratios. Hence, keel melt may be a significant additional factor in driving detachment events.

The phenomenon common to all 5 detachments is the flickering observed in the animated radar imagery, which is interpreted to be a manifestation of small-scale vibrational rotation or tilting of ice floes (Section 4.6).

Such behavior would be indicative of ice that is not secured to the seabed or the surrounding landfast ice, which is commensurate with the observation of subsequent ice motion. The underlying cause of this small-scale ice motion is not clear, but the lack of correlation with any local atmospheric observations suggests an oceanic origin. Shapiro (1987) suggests the passage of waves through the water beneath the ice causes floes to vibrate. Here, we propose flickering could arise from the motion of keels within the walls of their gouges following uplift through melt, repacking or a rise in sea level. Repacking itself would also be likely to cause changes in backscatter, especially in the sail. However, as described in Section 4.6, only one brief period of flickering was observed while the seafloor pressure gauge was operational and this did not coincide with any of the episodes of high-frequency variability or any other notable feature of the pressure or temperature records. Although it seems clear that flickering indicates that landfast ice is in the process of detaching from the coast, the data acquired in this study do not allow us to say what causes the ice to decouple from the seabed.

6. Conclusions

Development of the landfast ice at Barrow was markedly different between the two annual cycles observed in this study and the resulting ice covers differed from each other in appearance and anchoring strength. In 2003–04 the landfast ice near Barrow contained only a few small and discontinuous grounded pressure ridges. In 2004–05, by comparison, the landfast ice was dominated by a zone of large, continuous grounded shear ridges. Near-shore sea ice motion during the emplacement of landfast ice was qualitatively different between these two annual cycles as were the local winds during the formation period. However, ice motion in the radar data did not correlate with local wind observations and therefore the difference in winds of uncertain significance.

As a result of the difference in grounded ridge distributions, the landfast ice in 2004–05 was attached to the coast with an anchoring strength more than an order of magnitude greater than that in 2003–04. Although grounded ridges can anchor surrounding ice, form drag of their keels increase the water stress from under-ice currents. Ungrounded or weakly grounded ridges may therefore decrease the overall stability of the landfast ice. We speculate that numbers of grounded ridges intermediate between those in 2003–04 and those in 2004–05 may not be stable. Despite the difference in anchoring strengths, the overall landfast ice extent was similar between the two years.

This supports Mahoney et al.'s (in press) observation that landfast ice extent is determined primarily by the coastline and bathymetry. Detailed examination of five detachment events captured by the radar suggests that short-term local meteorological conditions are of little predictive use. Although under-ice currents were present during these events, estimates of the associated water stress were orders of magnitude less than the calculated anchoring strengths. Therefore, other processes must also act to decouple the grounded ridges or reduce their anchoring ability. These probably include sea level surges and, particularly in spring, surface melting of sails and thermal erosion of keels. Whatever the ultimate cause, the process of decoupling from the bed appears to cause target flickering in the radar imagery before ice motion. This suggests decoupling is a gradual process and should therefore be predictable on the timescale of hours. Towards this, we propose a simple technique to automatically detect the occurrence of flickering in radar data between 30 min and several hours prior to ice motion. However, since flickering is not always a precursor to ice motion, we recommend further work be carried out including the deployment of under-ice instruments to measure sea level, currents and water temperature.

Having stated that local meteorological observations are not useful for short-term prediction of landfast ice detachment, we should stress that landfast ice stability is affected by atmospheric forcing over longer time periods. Mahoney et al. (in press) found that the onset of thawing mean daily air temperatures preceded spring break-up by an average of 18 days between 1997 and 2004. This underscores the important role of melting in pre-conditioning the ice prior to offshore forcing at the end of the annual cycle. However, the two detachments events in March, 2004 were not preceded by thawing air temperatures and instead seem to have been driven purely by oceanic forcing.

Overall, these conclusions bring us closer to the level of understanding held by the members of indigenous communities along the Arctic Coast who have spent a lifetime studying landfast ice. The properties and processes that we have identified as vital for understanding the short-term stability of the ice are the same as those watched carefully by hunters while they are on the ice. Land-based radar offers an additional method of observing the ice and has been central to the discussion in this paper. In view of this, a new system has been installed offering both greater range and greater backscatter resolution. In addition, there is greater community awareness of the data and it is hoped that with the involvement of indigenous experts, some of the questions left unanswered in this study will be resolved.

Acknowledgements

This study was funded in part by the Center for Global Change Student Research Grant Competition (2003) and the National Science Foundation (OPP-9910888). We are very grateful to the Barrow Arctic Science Consortium and the Ukpeagvik Iñupiat Corporation Science Division, especially Robert Bulger (BASC) and Anne Jensen (UIC), for helping keep the radar running as continuously possible. The bathymetry survey would not have been possible without generous support from the North Slope Borough Department of Wildlife Management, particularly Dr. Craig George. We would also like to acknowledge advice from Dr. Ryan Phillips regarding seafloor gouging forces.

References

Aoki, S., Ozawa, T., Doi, K., Shibuya, K., 2000. GPS observation of the sea level variation in Ltzow-Holm Bay, Antarctica. Geophysical Research Letters 27, 2285–2288.

Bates, H.F., Shapiro, L., 1980. Long-period gravity waves in ice-covered seas. Journal of Geophysical Research 85, 1095–1100.

Been, K., Kosar, K., Hachey, J., Rogers, B.T., Palmer, A., 1990. Ice Scour Models, 9th International Conference on Offshore Mechanics and Arctic Engineering, vol. 5. American Society of Mechanical Engineers, Houston, TX, pp. 179–188. Feb 18–23, 1990.

Blanchet, D., 1998. Ice loads from first-year ice ridges and rubble fields. Canadian Journal of Civil Engineering 25, 206–215.

Cole, D.M., Eicken, H., Frey, K., Shapiro, L.H., 2004. Observations of banding in first-year Arctic sea ice. Journal Geophysical Research 109. doi:10.1029/2003JC001993.

Croasdale, K.R., Bruneau, S., Christian, D., Crocker, G., English, J., Metge, M., Ritch, R., 2001. In-Situ Measurements on the Strength of First-Year Ice Ridge Keels. 16th International Conference on Port and Ocean Engineering Under Arctic Conditions, Ottawa, Canada, August 12–17, 2001, vol. 3, pp. 1445–1454.

Croasdale, K.R., Comfort, G., Been, K., 2005. Investigation of ice limits to ice gouging. 18th International Conference on Port and Ocean Engineering Under Arctic Conditions, POAC '05, Clarkson University, Potsdam, NY, June 26–30, 2005. 1, pp. 43−52.

Eicken, H., Tucker, W.B.I., Perovich, D.K., 2001. Indirect measurements of the mass balance of summer Arctic sea ice with an electromagnetic induction technique. Annals of Glaciology 33, 194–200.

Fox, S., 2002. In: Krupnik, I., Jolly, D. (Eds.), These Are Things That Are Really Happening: Inuit Perspectives on the Evidence and Impacts of Climate Change in Nunavut. Arctic Research Consortium of the United States, Fairbanks, pp. 13–53.

George, J.C., Huntington, H.P., Brewster, K., Eicken, H., Norton, D.W., Glenn, R., 2004. Observations on shorefast ice dynamics in Arctic Alaska and the responses of the Iñupiat Hunting Community. Arctic 57, 363–374.

Haas, C., Eicken, H., 2001. Interannual variability of summer sea ice thickness in the Siberian and Central Arctic under different atmospheric circulation regimes. Journal of Geophysical Research 106, 4449–4462.

Hallikainen, M., Winebrenner, D.P., 1992. The Physical Basis for Sea Ice Remote Sensing. In: Carsey, F.D. (Ed.), Geophysical Monograph, vol. 68. American Geophysical Union, Washington, pp. 29–46.

Haykin, S., Lewis, E.O., Raney, R.K., Rossiter, J.R., 1994. Remote Sensing of Sea Ice and Icebergs. John Wiley and Sons, Inc., New York, NY.

Høyland, K.V., 2002. Consolidation of first-year sea ice ridges. Journal of Geophysical Research 107. doi:10.1029/2000JC000526.

Høyland, K.V., Løset, S., 1999. Measurements of temperature distribution, consolidation and morphology of a first-year sea ice ridge. Cold Regions Science and Technology 29, 59.

Jolly, D., Berkes, F., Castledon, J., Nichols, T., and the community of Sachs Harbor, 2002. In: Krupnik, I., Jolly, D. (Eds.), We Can't Predict the Weather Like We Used To: Inuvialuit Observations of Climate Change, Sachs Harbor, Western Canadian Arctic in The Earth Is Faster Now: Indigenous Observations of Arctic Environmental Change. Arctic Research Consortium of the United States, Fairbanks, AK.

Kovacs, A., Mellor, M., 1974. Sea Ice Geomorphology and Ice as a Geologic Agent in the Northern Beaufort Sea. In: Reed, J.C., Sater, J.E. (Eds.), The Coast and Shelf of the Beaufort Sea. Arctic Institute of North America, Arlington, VA, pp. 113–162.

Kovacs, A., Sodhi, D., 1988. Onshore ice ridge-up and pile-up: observations from theoretical assessment. In: Chen, A.T., Leidersdorf, P. (Eds.), Arctic Coastal Processes and Slope Protection, Reston, VA, American Society of Civil Engineers, ASCE Technical Council on Cold Regions, pp. 108–142.

Langleben, M.P., 1982. Water drag coefficient of first-year sea ice. Journal of Geophysical Research 87, 573–578.

Leppäranta, M., Hakala, R., 1992. The structure and strength of first-year ice ridges in the Baltic Sea. Cold Regions Science Technology 20, 295–311.

Leppäranta, M., Lensu, M., Kosloff, P., Veitch, B., 1995. The life story of a first-year sea ice ridge. Cold Regions Science and Technology 23, 279.

MacDonald, T., 2002. Ice floe breaks: 58 whalers flown to safety. The Arctic Sounder, Barrow, Alaska, 16, No. 21, pp. 1–8.

Mahoney, A. (2006), Alaska Landfast Sea Ice Dynamics, Ph. D. thesis, 152 pp, University of Alaska Fairbanks, Fairbanks, AK.

Mahoney, A., Eicken, H., Shapiro, L.H., Grenfell, T.C., 2004. Ice motion and driving forces during a spring ice shove on the Alaskan Chukchi Coast. Journal of Glaciology 50, 195–207.

Mahoney, A., Eicken, H., Shapiro, L., Graves, A., 2005. Defining and locating the seaward landfast ice edge in Northern Alaska. 18th International Conference on Port and Ocean Engineering under Arctic Conditions, POAC '05. Potsdam, N.Y., June 26–30, 2005. 3, pp. 100−109.

Mahoney, A., Eicken, H., Shapiro, L., Gaylord, A., in press. Alaskan landfast sea ice: links with bathymetry and atmospheric circulation, Journal of Geophysical Research.

Marchenko, A., 2003. Modelling of the formation of long grooves in the seabed by grounded ice keels. Journal of Ship and Ocean Technology 7, 1–15.

Marchenko, A., 2005. Forming of seabed scours by tidal drift of a floe joined to a grounded ridge. 18th International Conference on Port and Ocean Engineering Under Arctic Conditions, POAC '05. Clarkson University, Potsdam, NY, June 26-30, 2005. 1, p. 53−64.

Marsden, R.F., Paquet, R., Ingram, R.G., 1994. Currents under landfast ice in the Canadian Arctic Archipelago. Part 1: vertical velocities. Journal of Marine Research 52, 1017–1036.

Maykut, G.A., 1986. In: Untersteiner, N. (Ed.), The Surface Heat and Mass Balance. Martinus Nijhoff Publ., Dordrecht, pp. 395–463. NATO ASI B146.

Norton, D.W., Graves Gaylord, A., 2004. Drift velocities of ice floes in Alaska's northern Chukchi Sea flaw zone: determinants of success by spring subsistence whalers in 2000 and 2001. Arctic 57, 347–362.

Perovich, D.K., Grenfell, T.C., Richter-Menge, J.A., Light, B., Tucker III, W.B., Eicken, H., 2003. Thin and thinner: sea ice mass balance measurements during Sheba. Journal of Geophysical Research 108. doi:10.1029/2001JC001079.

Phillips, R., Clark, J.I., Kenny, S., 2005. PRISE Studies on Gouge Forces and Subgouge Deformations. 18th International Conference on Port and Ocean Engineering Under Arctic Conditions, POAC '05, Clarkson University, Potsdam, NY, June 26–30, 2005, vol. 1, pp. 75–84.

Pilkington, G.R., O'Rourke, J.C., Steen, J.W., Banke, E.G., 1980. Ridge Keel Observations, Workshop on Sea Ice Ridging and Pile-up, National Research Council, Associate Committee on Geotechnical Research, Technical Memorandum, no. 134, Calgary, Alberta, October 22–24, 1980.

Reimnitz, E., 2000. Interactions of river discharge with sea ice in proximity of Arctic deltas: a review. Polarforschung 70, 123–134.

Reimnitz, E., Barnes, P., 1974. In: Reed, J.C., Slater, A.G. (Eds.), Sea Ice as a Geologic Agent on the Beaufort Sea Shelf of Alaska, in The Coast and Shelf of the Beaufort Sea (Proceedings of a Symposium on Beaufort Sea Coast and Shelf Research). Arctic Institute of North America, Arlington, VA, pp. 301–353.

Serreze, M.C., Maslanik, J.A., Scambos, T.A., Fetterer, F., Stroeve, J., Knowles, K., Fowler, C., Drobot, S., Barry, R.G., Haran, T.M., 2003. A record minimum Arctic sea ice extent and area in 2002. Geophysical Research Letters 30, 1110. doi:10.1029/2002GL016406.

Shapiro, L.H. (1987), Mechanical Properties of Sea Ice Deformation in the near Shore Zone, in OCSEAP Final Reports, V.72, edited, pp. 357–584, U.S. Dept. of Commerce, NOAA.

Shapiro, L.H., Barnes, P.W., 1991. Correlation of nearshore ice movement with seabed ice gouges near Barrow, Alaska. Journal Geophysical Research 96, 16979–16989.

Shapiro, L., Metzner, R., 1987. Coefficients of friction of sea ice on beach gravel. Journal of Offshore Mechanics and Arctic Engineering 109, 388–390.

Shirasawa, K., 1986. Water stress and ocean current measurements under first-year sea ice in the Canadian Arctic. Journal of Geophysical Research 91, 14, 305–14, 316.

Stroeve, J.C., Serreze, M.C., Fetterer, F., Arbetter, T., Meier, W., Maslanik, J., Knowles, K., 2005. Tracking the Arctic's shrinking ice cover: another extreme September minimum in 2004. Geophysical Research Letters 32, L04501. doi:10.1029/2004GL021810.

Timco, G.W., Burden, R.P., 1997. An analysis of the shape of sea ice ridges. Cold Regions Science and Technology 25, 65–77.

Weeks, W.F., 1985. The variation of ice strength within and between multiyear pressure ridges in the Beaufort Sea. Journal of Energy Resources Technology 107, 167–172.

Weeks, W.F., Ackley, S.F., 1986. In: Untersteiner, N. (Ed.), The Growth, Structure and Properties of Sea Ice. Plenum Press, New York, pp. 9–164. NATO ASI B146.